Calculation of Axisymmetric, Turbulent, Confined Diffusion Flames

S. P. Vanka*
Argonne National Laboratory, Argonne, Illinois

A solution algorithm based on a fully coupled solution of the time-averaged Navier-Stokes equations is developed for the calculation of turbulent reacting flows. The governing elliptic partial differential equations are discretized by finite differences and the nonlinear algebraic equations are solved by a block-implicit algorithm employing Newton's method and sparse matrix techniques. Calculations have been made of a confined turbulent diffusion flame. Turbulence is represented by the $k\sim\epsilon$ model and chemical reaction is assumed to occur in one step at an infinite rate, controlled by the mixing of fuel and oxidant streams. It is demonstrated that the strategy of a coupled solution is rapidly convergent even in the presence of significant density variations. Calculations with finite difference grids as large as 80×100 have been made successfully in modest computer time and with modest storage. The calculations are compared with experimental data.

Nomenclature

a = coefficients in the finite difference equations; also used for parameter in β function pdf
A = area of cell faces
b = parameter in β function
C_p = specific heat
F = column vector of residual functions
h = enthalpy of mixture
H_{fu} = heat of reaction
k = kinetic energy of turbulence
m = mass fraction
M = molecular weight
p = pressure
P = Peclet number
Q = general property function
r = radial distance
R = gas constant
s = streamline coordinate
$S,\bar{S}$ = source terms in differential and finite difference equations, respectively
T = temperature
u,v = x- and r-direction velocity components, respectively
V = volume of finite difference cell
x = axial coordinate distance
X = column vector of updates to dependent variables
α = relaxation factor on density
Γ = exchange coefficient
ϵ = rate of dissipation of turbulence energy
$\partial F/\partial X$ = Jacobian matrix of finite difference equations
ξ = nondimensional mixture fraction
$\bar{\xi},\overline{\xi'^2}$ = mean and variance of nondimensional mixture fraction
ρ = mixture density
Φ = mixture fraction

Subscripts

A = airstream
F = fuel stream
fu = fuel
ox = oxidant
pr = product
x,r = axial and radial coordinates
P = point P in the finite difference grid
ϕ = general flow variable

Presented as Paper 85-0141 at the AIAA 23rd Aerospace Sciences Meeting, Reno, NV, Jan. 14-17, 1985; received Jan. 30, 1985; revision received July 1, 1985.

*Mechanical Engineer, Components Technology Division. Member AIAA.

Introduction

RECENTLY there have been a number of research efforts toward the development of mathematical models for turbulent reacting flows. Such studies have been motivated by the need to understand and predict the combustion processes in devices such as gas turbine and ramjet combustors,[1-5] liquid- and gaseous-fueled furnaces,[6-9] chemical lasers, and other propulsion devices such as ducted rockets.[10] In these studies the approach has been to numerically solve a set of nonlinear partial differential equations that govern the time-averaged multidimensional transport of mass, momenta, and chemical species. To close the equation set, closure hypotheses for turbulence (such as the $k\sim\epsilon$ model[11]) and turbulence/chemistry interaction (such as the eddy-breakup model[12]) are employed.

The task of numerically solving such a set of equations is large and complex because the equations are nonlinear and strongly coupled through interactions between pressure, velocity, turbulence, and temperature. The equations are elliptic in space, characterizing regions of flow recirculation. Further, the equations governing the commonly used turbulence quantities, such as the kinetic energy of turbulence and its dissipation rate, are highly nonlinear because of their stiff source terms and coupling.

The present paper is concerned with the development of an efficient solution algorithm for the equations of a turbulent reacting flow. The present procedure differs from several others currently in use (notably, SIMPLE[13] and its variants) by employing a coupled solution of the momentum and continuity equations. In recent works of the author,[14,15] it was observed that such a simultaneous solution of the momentum and continuity equations has several advantages. Specifically, it was observed that, for the calculation of isothermal flows, the procedure is 1) rapidly convergent to very low residuals in a few iterations, 2) insensitive to variations in the parameters of the finite difference grid such as the number of nodes and cell aspect ratios, and 3) satisfactorily convergent without the use of underrelaxation factors commonly necessary in earlier procedures.

The work described herein is an extension of the coupled solution methodology to the set of equations describing a chemically reacting flow. The additional complexity introduced is the (strong) variation in fluid density resulting from chemical reaction. Calculations have been made of a turbulent confined diffusion flame typical of gaseous-fueled furnaces. The turbulence is modeled by the $k\sim\epsilon$ turbulence model,[11] and, for simplicity, the chemical reaction is considered to be mixing-limited.[16] The time-mean mixture properties are obtained by convoluting the property functions with a β probability density function (pdf). Additional partial differential equations are solved for the mean and variance of a conserved scalar (ξ) defined as

$$\xi=\frac{\Phi-\Phi_A}{\Phi_F-\Phi_A} \tag{1}$$

where $\Phi=m_{\rm fu}-m_{\rm ox}/i$ and $m_{\rm fu}$, $m_{\rm ox}$, and i represent mass fractions of fuel and oxidant, and their stoichiometric ratio, respectively. The following sections describe the details of the calculation procedure and its performance. The calculations are compared with experimental data to evaluate the accuracy of the closure models.

Equations Solved

General Form

The set of equations solved here describes the steady-state transport of mass, momentum, and chemical species in an axisymmetric reacting flow. A total of seven partial differential equations are solved to evaluate the unknown variables u, v, p, k, ϵ, $\bar{\xi}$, and $\overline{\xi'^2}$ representing the two velocities, the pressure, the kinetic energy of turbulence and its dissipation rate, and the mean and variance of the conserved scalar. The set of partial differential equations has the following general form:

$$\frac{\partial}{\partial x}(\rho u\phi)+\frac{\partial}{r\partial r}(\rho rv\phi)=\frac{\partial}{\partial x}\left(\Gamma_\phi\frac{\partial\phi}{\partial x}\right)+\frac{\partial}{r\partial r}\left(r\Gamma_\phi\frac{\partial\phi}{\partial r}\right)+S_\phi \tag{2}$$

where Γ_ϕ and S_ϕ are exchange coefficients and source terms in the appropriate equations. The expressions for Γ_ϕ and S_ϕ for the seven equations are quoted in several earlier works and are given in Table 1 of Ref. 20.

The properties of the reacting mixture are evaluated by convoluting the property functions with a β probability density distribution. Specifically, any mixture property, $\bar{Q}$, is evaluated from the expression

$$\bar{Q}=\int_0^1 Q(\xi)\xi^{a-1}(1-\xi)^{b-1}\mathrm{d}\xi\Big/\int_0^1\xi^{a-1}(1-\xi)^{b-1}\mathrm{d}\xi \tag{3}$$

where ξ is the instantaneous mixture fraction. Q represents (density)$^{-1}$, temperature, enthalpy, etc. The parameters a and b are calculated from the local values of $\bar{\xi}$ and $\overline{\xi'^2}$ from the relations

$$a=\bar{\xi}\left\{\frac{(1-\bar{\xi})\bar{\xi}}{\overline{\xi'^2}}-1\right\}\qquad b=\frac{(1-\bar{\xi})}{\bar{\xi}}a \tag{4}$$

The property functions for the mixture are prescribed from the following relations for an adiabatic flow:

$$h(\xi)=\xi h_F+(1-\xi)h_A \tag{5}$$

$$T(\xi)=\frac{h(\xi)-m_{\rm fu}H_{\rm fu}}{\bar{C}_p(\xi)} \tag{6}$$

$$\bar{C}_p(\xi)=\sum_i m_i(\xi)C_{p_i}(\xi) \tag{7}$$

$$\rho(\xi)=\frac{M(\xi)p}{RT(\xi)} \tag{8}$$

and

$$\frac{1}{M(\xi)}=\frac{m_{\rm fu}(\xi)}{M_{\rm fu}}+\frac{m_{\rm ox}(\xi)}{M_{\rm ox}}+\frac{m_{\rm pr}(\xi)}{M_{\rm pr}} \tag{9}$$

The symbols used are explained in the nomenclature. The subscript i in Eq. (7) refers to fuel, oxidant, and product fractions of the mixture.

Boundary Conditions

The boundary conditions for the preceding set of equations depend on the geometry of the flow situation. Both Dirichlet and Neumann boundary conditions can be employed, although an additional equation for enthalpy is needed for nonadiabatic situations. Near solid walls, because of steep property variations, "wall functions" have been employed to obtain more realistic shear stresses. Details of the boundary conditions for the present calculations are given in a later section.

Finite Differencing

The discrete forms of the governing equations are derived by integrating the equations locally over finite "control volumes." A staggered mesh system[13] is used to locate the flow variables on a finite difference grid network formed by lines of constant x and r coordinates. The velocities are located between the pressures. The internode variation of the dependent variable is obtained from the solution of the locally one-dimensional transport equation

$$\rho u_s\frac{\partial\phi}{\partial s}-\Gamma_\phi\frac{\partial^2\phi}{\partial s^2}=0 \tag{10}$$

where ϕ denotes any one of the variables and s is one of the two coordinate directions. The solution to the above equation is an exponential relation of ϕ with s, given by

$$\phi=\phi_1+(\phi_2-\phi_1)(e^{P\eta}-1)/(e^P-1) \tag{11}$$

where

$$P=\rho u_s(s_2-s_1)/\Gamma_\phi \tag{12}$$

and

$$\eta=(s-s_1)/(s_2-s_1) \tag{13}$$

The symbols s_2 and s_1 denote the distance of integration.

The integration of the convective and diffusive operators amounts to the algebraic summation of the fluxes on the faces of the control volumes. For a flow variable denoted by the general symbol ϕ, the discrete equation can be written as

$$\begin{aligned}&(\rho u\phi)_{x^+}A_{x^+}-(\rho u\phi)_{x^-}A_{x^-}+(\rho u\phi)_{r^+}A_{r^+}-(\rho u\phi)_{r^-}A_{r^-}\\&=\Gamma_{x^+}\left(\frac{\partial\phi}{\partial x}\right)_{x^+}A_{x^+}-\Gamma_{x^-}\left(\frac{\partial\phi}{\partial x}\right)_{x^-}A_{x^-}\\&+\Gamma_{r^+}\left(\frac{\partial\phi}{\partial r}\right)_{r^+}A_{r^+}-\Gamma_{r^-}\left(\frac{\partial\phi}{\partial r}\right)_{r^-}A_{r^-}+\int S_\phi\mathrm{d}V\end{aligned} \tag{14}$$

After the internodal variations are incorporated and like terms are collected, the finite difference equations can be written, in an abbreviated form, as

$$a_P\phi_P=\sum_i a_i\phi_i+\bar{S} \tag{15}$$

where the expressions for a contain velocities, diffusion coefficients, and cell dimensions. $\bar{S}$ is the integrated source term. P refers to the value at the cell and the summation is over the neighboring values.

The above integration methodology has been widely used; for example, in Ref. 13. It has the merits of physical realism and simplicity. However, more accurate finite differencing schemes can also be used. The form of the solution procedure, however, will remain invariant under other discretization procedures.

Solution Algorithm

General Features

The solution of the large set of nonlinear algebraic equations obtained after discretization is a difficult task even with the availability of fast computers. A problem of great concern is the rate and certainty of convergence of the solution process starting from an initially guessed distribution of flow variables. The strong coupling between the velocity and pressure fields and the nonlinear stiff source terms in the turbulence equations has a dominant influence on the solution strategy. In several earlier works these equations are solved in an iterative sequence in which the equations are solved individually with the coefficients evaluated from previous iterate values. Because of the decoupling and the specific manner of linearization, such procedures frequently require under-relaxation of the variables in order to maintain numerical stability. Also, the convergence of such procedures is sensitive to parameters such as flow Reynolds numbers, grid density, and grid aspect ratio.

In his recent work,[14,15] the author has observed that a coupled solution of the momentum and continuity equations is rapidly convergent and requires significantly less computer time. Such a coupled solution eliminates the need for the transformation of the continuity equation into a pressure or pressure-correction equation; rather, the continuity equation is differenced and solved in its primitive form. The coupled approach leads to a blocked nonlinear equation set with a block size equal to the number of partial differential equations. The blocked equations are solved by Newton's method with direct inversion of the Jacobian. The storage requirements are reduced significantly and made manageable through techniques such as preordering the equations and splitting the flow region into smaller domains.

The turbulence equations are solved decoupled from the momentum equations but still within the Newton's iteration loop. The equations for k and ϵ are solved by a line-by-line algorithm until the residuals have decreased to very low values. The turbulent viscosity is then updated for use in the subsequent solution of the momentum equations. For the present case of reacting flows, an additional nonlinearity arises from the variation of density as a function of the mean and variance of the conserved scalar. In the present work, the equations for $\bar{\xi}$ and $\overline{\xi'^2}$ are solved inside the overall Newton's loop, after the equations for k and ϵ have been solved. The time-mean density is then evaluated by convoluting the density function with a β pdf.

The complete details of the present method are given below.

Solution of the Momentum and Continuity Equations

The solution of the momentum and continuity equations is the first phase of calculation at each iteration in the overall iterative sequence. The finite-differenced momentum and continuity equations at any node symbolically represented by P are as follows:

$$a_P^u u_P = \Sigma a_i^u u_i + (p_{x^-} - p_{x^+}) V^u / \Delta x^u \tag{16}$$

$$a_P^v v_P = \Sigma a_i^v v_i + (p_{r^-} - p_{r^+}) V^v / \Delta r^v \tag{17}$$

and

$$\rho_{x^+} A_{x^+} u_{x^+} - \rho_{x^-} A_{x^-} u_{x^-} + \rho_{r^+} A_{r^+} v_{r^+} - \rho_{r^-} A_{r^-} v_{r^-} = 0 \tag{18}$$

In vector form, they can be written as

$$F(X) = 0 \tag{19}$$

$$[X] = [X_{11}, X_{12}, \ldots, X_{21}, X_{22}, \ldots]^T \tag{20}$$

$$[F] = [F_{11}, F_{12}, \ldots, F_{21}, F_{22}, \ldots]^T \tag{21}$$

$$X_{ij} = (u, v, p)_{ij}^T \tag{22}$$

and

$$F_{ij} = (F^u, F^c, F^v)_{ij}^T \tag{23}$$

F is a large set of nonlinear functions expressing the residuals in the momentum and continuity equations, and the column vector X represents the unknown flow variables. The set of nonlinear equations is solved iteratively by Newton's method. At each iteration, the X vector is updated by

$$X_n = X_{n-1} - \left(\frac{\partial F}{\partial X}\right)_{n-1}^{-1} F_{n-1} \tag{24}$$

where n is the current iteration number and $(\partial F/\partial X)$ the Jacobian of the equation set. The structure of the Jacobian for a model grid is shown in Fig. 1.

The Jacobian for the present system is unsymmetric because of the first-order derivatives in some of the terms (e.g., convection and pressure gradients). Iterative inversion of the Jacobian may be unreliable and difficult to converge; therefore, a direct factorization procedure is used. The factorization is carried out without any pivoting, using an efficiently coded sparse matrix package.[17] The computer storage required by the factors is reduced by two other novel techniques integrated into the overall sequence, namely alternate diagonal ordering and domain splitting.[15] The alternate diagonal ordering is a preordering technique for the blocks of equations. Instead of ordering the grid nodes along one particular direction (as in grid row ordering), the alternate diagonal ordering numbers the blocks of equations on alternate diagonals, reducing the storage and computer time by a factor of 2-3.

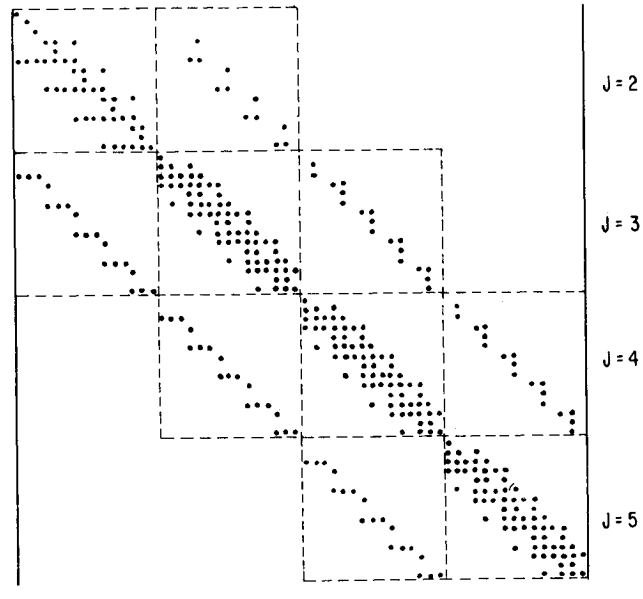

Fig. 1 Structure of the Jacobian matrix.

The domain-splitting technique, on the other hand, is a divide-and-conquer strategy. The flowfield is first divided into a small number of subdomains, as few as two or as many as ten. The subdomains are defined to be overlapping. The flow equations are then solved as follows. First, a sequence is defined for visiting each subdomain; this is done through the numbering of the subdomains. Each subdomain is solved with known conditions on its four boundaries. The boundary conditions may be fixed (such as at walls) or may be those obtained from an earlier solution of the neighboring subdomain. The Jacobian matrix of the coefficients is formulated only for the subdomain of current interest and the LU factorization is obtained for this limited region. Because the subdomains are considerably smaller than the complete domain, the storage occupied is now much smaller. The subdomain splitting has permitted calculations with finite difference grids as large as 80×100 with a modest amount of computer storage and time.

Solution of the Turbulence Equations

The primary difficulty in solving the turbulence equations is the stiff nonlinearity ($1/k$ variation) in the source term of the ϵ equation. Careful consideration must therefore be given to the handling of these stiff nonlinearities; otherwise k and ϵ may attain unphysical values. The difficulties in the solution arise primarily from regions of high shear where the source terms are predominant, and the initial guess to the values of k and ϵ are generally in error.

The approach followed in this study is identical to the one used successfully in the calculation of isothermal flows, described in Ref. 14. Briefly, the features are: 1) the k and ϵ equations are solved separate from the momentum and continuity equations, but within the outer Newton's iteration; 2) emphasis is placed on obtaining an accurate solution of the k and ϵ fields before the next update of the velocities; and 3) the k and ϵ equations are solved by a line-by-line marching procedure and, at each line, the equations are solved repeatedly until a specified accuracy (1.0×10^{-4}) is reached.

Solution of the Scalar Transport Equations

The equations for the transport of the mean and variance of the mixture fraction ($\bar{\xi}$, $\overline{\xi'^2}$) are linear for given velocity and concentration fields. Therefore, their solution is not as difficult as those for the transport of k and ϵ. Nevertheless, because the density and temperature are evaluated from the distributions of $\bar{\xi}$ and $\overline{\xi'^2}$, it is necessary that these be calculated accurately. In the present work, the two equations are solved sequentially by an alternating-direction line-elimination algorithm. The equation for $\bar{\xi}$ is satisfied and the new distribution of $\bar{\xi}$ is subsequently used in evaluating the production of concentration fluctuations. New fields of mixture density and temperature are evaluated from values of $\bar{\xi}$ and $\overline{\xi'^2}$. The evaluation of the mixture properties in conjunction with a pdf is described in detail in Ref. 20.

Application and Results

Geometry Considered

A number of earlier studies[6-8] have been concerned with the measurement of mean flow properties of axisymmetric confined diffusion flames. In these experiments, the fuel and air entered as coaxial jets into a suddenly expanding chamber, simulating an industrial furnace. Measurements were made primarily of mean species, concentrations, and temperatures, but in some cases velocities were also measured. A detailed examination of available experiments for validation of turbulence and combustion models has been made recently under the NASA-HOST aerothermal modeling assessment program.[18,19]

In the present study, the geometry of Lockwood et al.[6] is selected for the purpose of demonstrating the calculation procedure. In these experiments coaxial streams of town gas and air are admitted into a cylindrical chamber (town gas as the inner stream). The flame is stabilized at the dividing lip between the two streams. Measurements have been made of the time mean mixture fractions $\bar{\xi}$ for different fuel/air ratios and with swirl in the airstream. The walls of the furnace are cooled by circulating water, although measurements of the wall temperature have not been reported. The effects of burner geometry, Reynolds number, and swirl are reported. In the present study only the nonswirling cases have been calculated for fuel/air ratios of 0.0785 and 0.0635. Complete details of the experiments can be obtained from Ref. 6.

Details of Computations

Calculations have been made with different finite difference grids to study the effects of grid fineness on the convergence of the algorithm and the accuracy of the finite differencing. The finite difference grids considered contained 40×19, 40×27, 80×64, and 80×97 grid nodes in the x and r directions, respectively. The grid nodes were nonuniformly distributed with aspect ratios varying between 5 and 20. The 40×19 grid node contained two nodes in the central jet and three nodes in the annular airstream. The 40×27 grid contained nine nodes in the central jet; the distribution of the remaining nodes was kept the same as the 40×19 grid. The 80×64 and 80×97 grids contained grid refinement in both the radial and axial coordinate directions. For the 40×19 and 40×27 grids, the complete domain was divided into four nearly equal subdomains. For the 80×64 and 80×97 grids eight subdomains were employed. The inlet profiles of the flow variables in the two streams were prescribed to correspond with fully developed flow in a straight pipe and an annulus, respectively. These conditions are consistent with the long settling lengths used in the experiments. At the exit, a zero derivative condition is used on the relevant flow variables. However, care is taken to preserve the overall mass continuity. A zero derivative boundary condition is also prescribed at the axis of symmetry. The walls are considered adiabatic. The values for the constants in the turbulence model are as follows. The fuel properties used are given in Table 1.

$$C_\mu=0.9,\quad C_1=1.47,\quad C_2=1.92,\quad C_{g1}=2.8,\quad C_{g2}=2.0$$

$$\sigma_k=1.0,\quad \sigma_\epsilon=1.3,\quad \sigma_f=0.6,\quad \sigma_g=0.6$$

For the present calculations it was not necessary to use any underrelaxation factors on the velocities, pressure, turbulence, and scalar variables. This experience is similar to that for isothermal flows. However, it was necessary to underrelax the successive changes in the density field slightly. A value of $\alpha=0.7$ was used in all calculations, with α defined as

$$\rho=\alpha\rho^{\text{new}}+(1-\alpha)\rho^{\text{old}} \tag{25}$$

Table 1 Fuel properties

Stoichiometric ratio:	10.59	
Heat of reaction:	2.630×10^7 J/kg	
Molecular weights:		
Air	28.82	
Fuel	10.18	
Products	25.69	
Specific heat (kJ/deg/kg) constants:		
	a_i	b_i
Air	1.00	1.21E−4
Fuel	2.11	1.67E−3
Products	1.08	2.71E−4

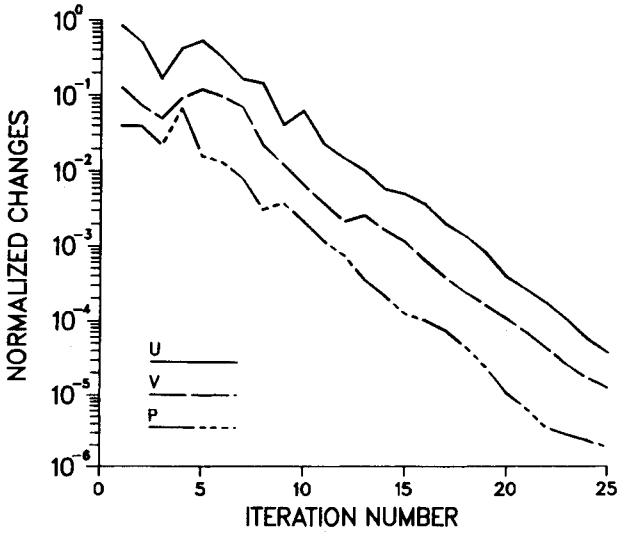

Fig. 2 Rate of convergence, 40×27 grid, $F/A = 0.0635$.

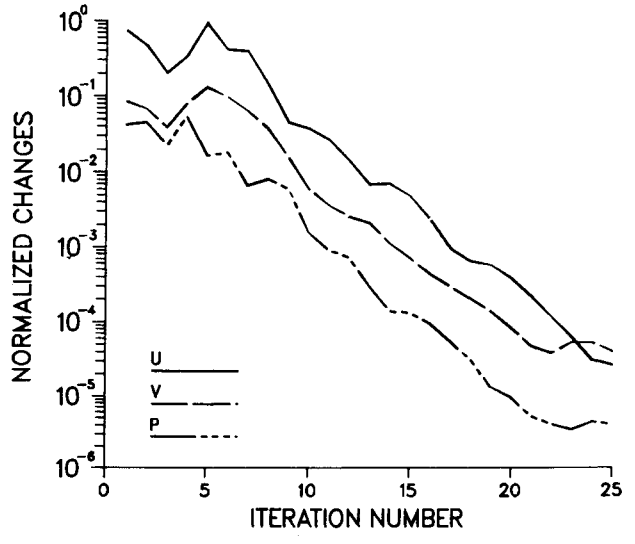

Fig. 3 Rate of convergence, 80×64 grid, $F/A = 0.0635$.

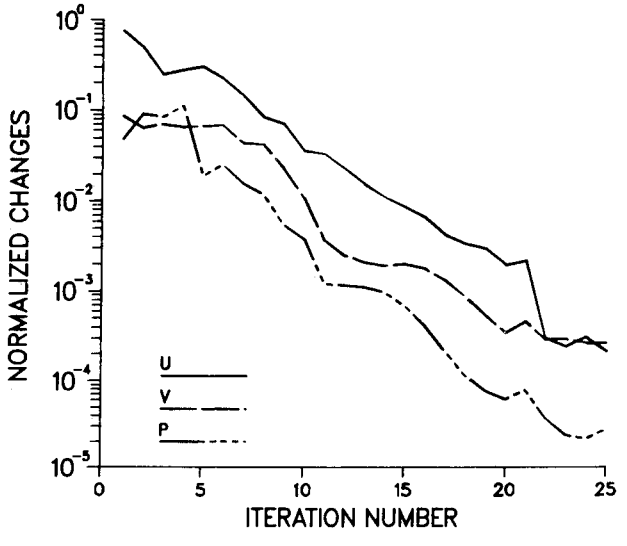

Fig. 4 Rate of convergence, 80×97 grid, $F/A = 0.0635$.

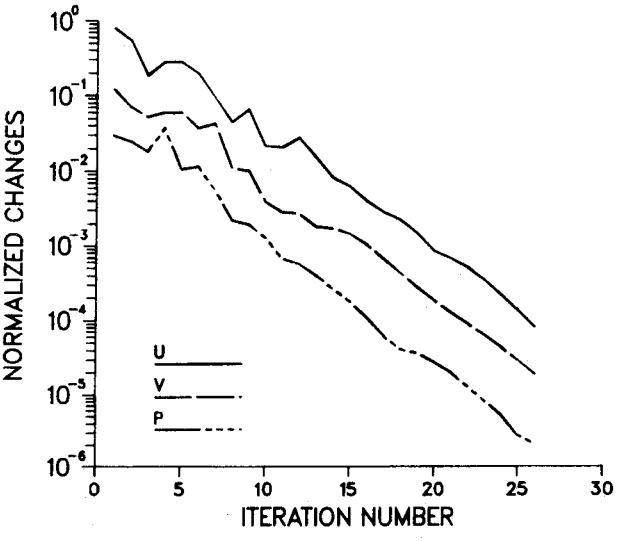

Fig. 5 Rate of convergence, 40×27 grid, $F/A = 0.0785$.

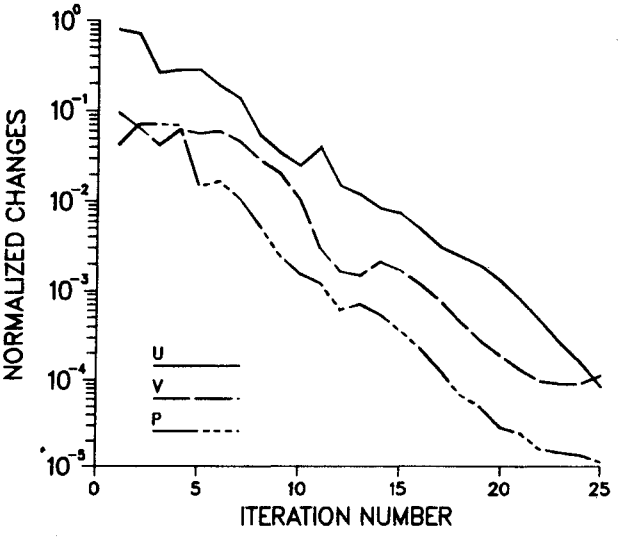

Fig. 6 Rate of convergence, 80×64 grid, $F/A = 0.0785$.

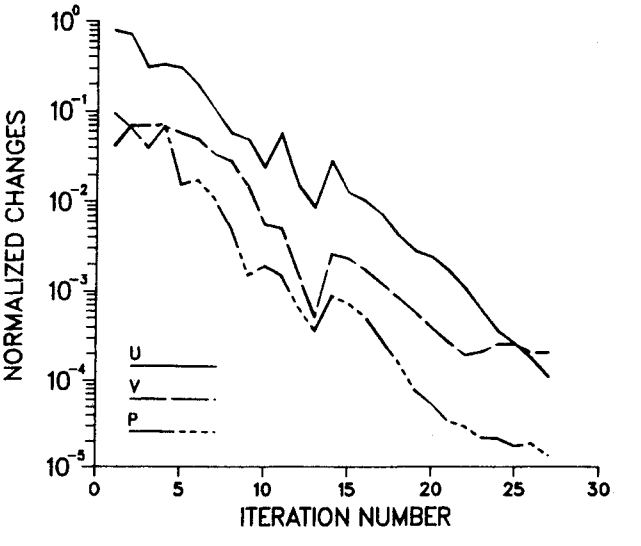

Fig. 7 Rate of convergence, 80×97 grid, $F/A = 0.0785$.

The value of α in current calculations is much larger than the values employed in earlier studies by the SIMPLE algorithm.[13]

Convergence Behavior

The merits of any algorithm are judged by two factors, namely 1) its rate of convergence, and 2) its robustness to changes in geometry, flow conditions, and finite difference grid. In this section the rates of convergence for the four finite difference grids and the two fuel/air ratios are presented. Figures 2-4 show the decrease of normalized successive changes in u, v, and pressure fields with iteration number for the fuel/air ratio of 0.0635. These changes may also be interpreted as the normalized residuals in the finite difference equations (the mass residual is always zero). It can be seen that the rate of convergence is fast for all of the grids, typically requiring only 25-30 iterations to achieve high accuracy. Further, the residuals decrease to small values without any sluggish behavior. The currently observed rates are similar to those for isothermal flows. Therefore, it is encouraging to observe that the algorithm retains its strength in the presence of strong density variations. The corresponding rates of convergence for the fuel/air ratio of 0.0785 are shown in Figs. 5-7. The impact of the fuel/air ratio on the convergence rate appears insignificant. The computer times required for these calculations on an IBM 3033 machine were as follows: 40×19 grid: 104 s; 40×27 grid: 150 s; 80×64 grid: 900 s; 80×97 grid: 1500 s.

Effect of Finite Difference Grid on Calculated Flowfields

The number of grid nodes and their locations in the computational domain play a central role in obtaining an accurate solution of the differential equations. The number of required grid nodes depends on the internal variations of the flow variables and the locations of the grid nodes. For example, two grids with the same total number of nodes but with one having more nodes placed in the thin shear layers may produce different results. Because of such difficulties, reports of past experiences are somewhat confusing. Elgobashi,[7] for example, reports that a 15×20 grid produces nearly the same results as a 20×30 grid. Smith and Smoot,[8] on the other hand, show a signficiant effect of the finite difference grid even for small changes in the number of grid nodes.

One of the objectives of the present study has been to investigate these grid dependency effects in more detail. The flow variables calculated with these grids are compared at several locations, especially in regions of steep variations. Some of these comparisons are presented in Figs. 8-10 for

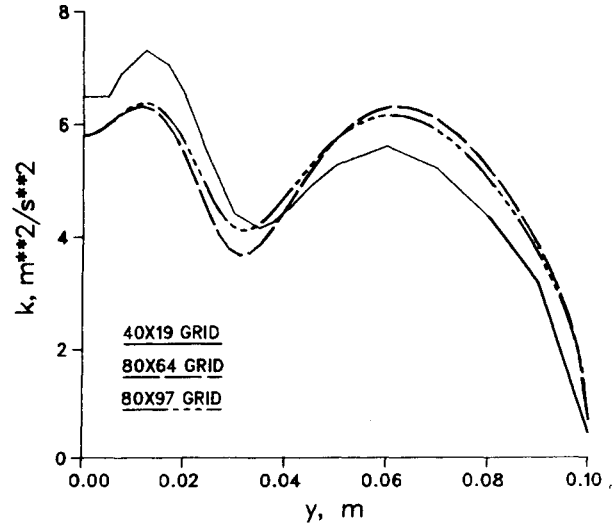

Fig. 9 Calculated radial profiles of turbulent kinetic energy at $x=0.39$ m.

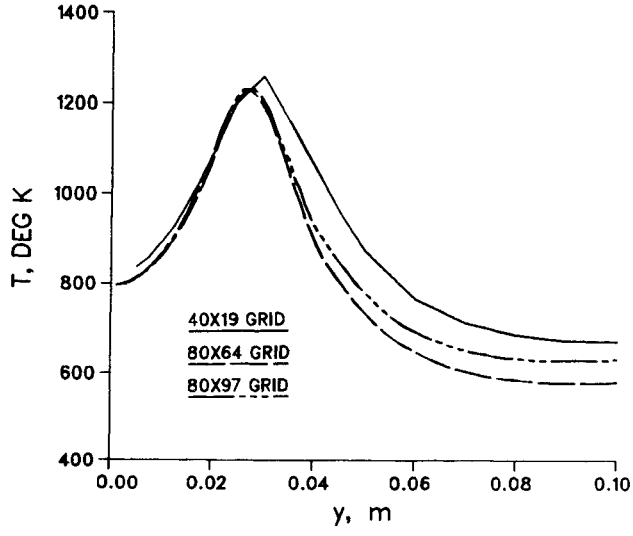

Fig. 10 Calculated radial profiles of temperature at $x=0.39$ m.

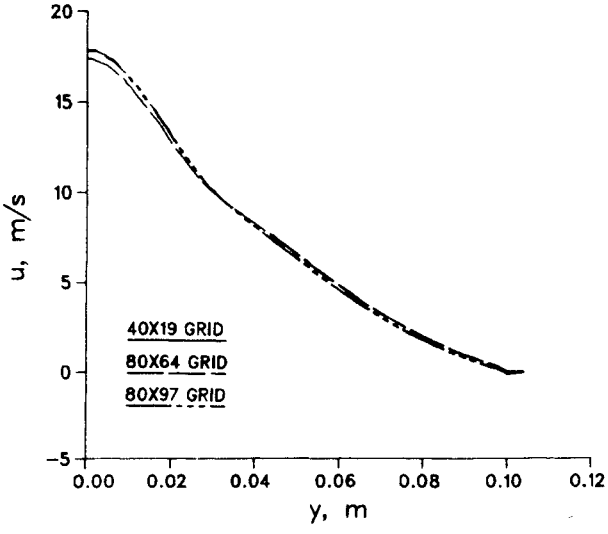

Fig. 8 Calculated radial profiles of u velocity at $x=0.38$ m.

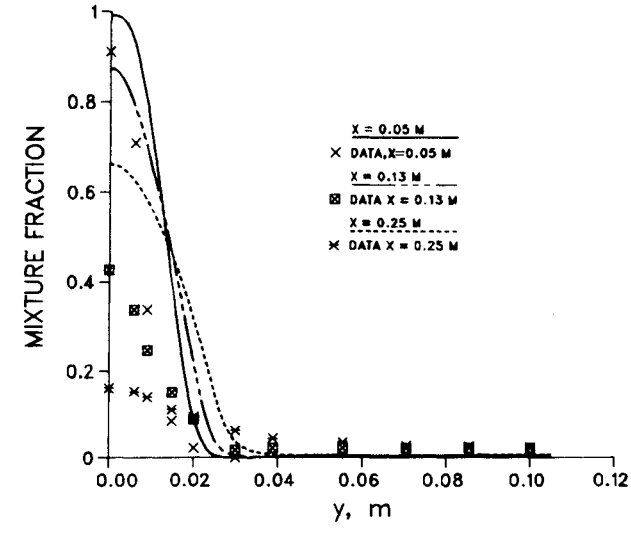

Fig. 11 Radial distribution of mixture fraction, $F/A=0.0635$.

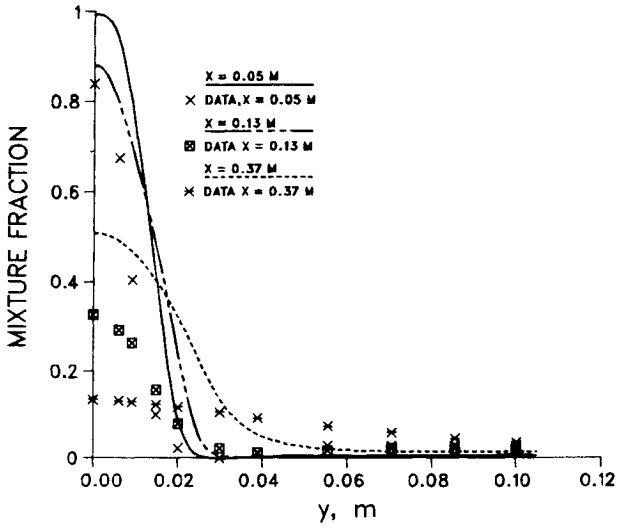

Fig. 12 Radial distribution of mixture fraction, $F/A = 0.0785$.

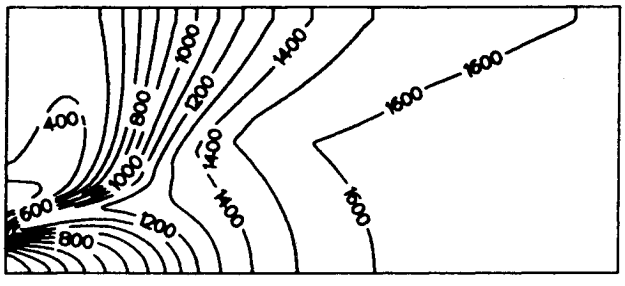

Fig. 13 Contours of temperature (°K), $F/A = 0.0785$.

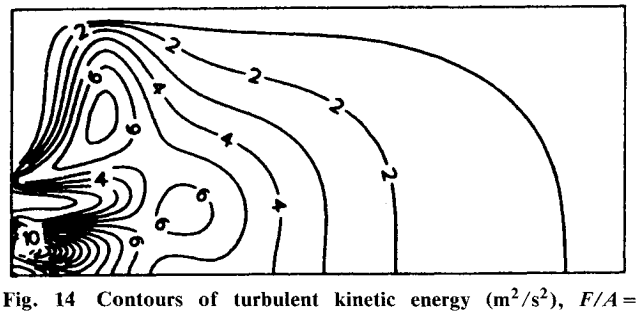

Fig. 14 Contours of turbulent kinetic energy (m^2/s^2), $F/A = 0.0785$.

the fuel/air ratio of 0.0785; comparisons of 0.0635 are similar.

From the preceding comparisons, it is evident that the 40×19 finite difference grid is not sufficient to adequately resolve the gradients in the shear layer. The 80×64 and 80×97 grids produce results in close agreement; therefore, it may be said that the 80×64 grid is adequate. It is necessary to caution here that such recommendations are somewhat subjective and depend on the quantity compared and the degree of accuracy desired. Also, if the differencing scheme is improved through the inclusion of higher-order terms, smaller grids may be adequate. An advantage of the present solution algorithm is that the finite difference equations on all grids can be solved efficiently to very low residuals, thereby removing the differences that usually result from incomplete convergence on fine grids.

Comparison with Experimental Data

Lockwood et al.[6] present distributions of time mean mixture fraction for different test conditions. In this section, we

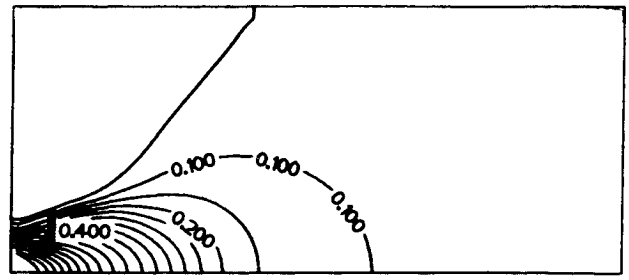

Fig. 15 Contours of nondimensional mixture fraction, $F/A = 0.0785$.

first compare the calculated mixture fraction distributions with measured values. Figure 11 compares the calculated radial profiles of mixture fraction at several axial locations for a fuel/air ratio of 0.0635. The calculated values have the same qualitative trends as the experimental values; however, significant quantitative differences exist. The calculated mixture fractions in the central jet region are higher than the data, indicating underexpansion of the central jet. Such discrepancies had also been reported earlier by Elgobashi[7] and Smith and Smoot,[8] albeit to a lesser extent, and are attributed to the inadequacies of the turbulence and combustion models. Figure 12 compares the calculated distributions of mixture fraction for the fuel/air ratio of 0.0785. The discrepancies are similar to those of a fuel/air ratio of 0.0635.

Figures 13-15 show the contours of temperature, turbulence kinetic energy, and mixture fraction (ξ) rate for a fuel/air ratio of 0.0785. These contours show the flame front and mixing layer of the fuel and airstreams. These plots agree qualitatively with earlier calculations, especially those of Elgobashi, and with experimental data.

To improve present calculations, it is possible to modify the $k \sim \epsilon$ model and the concentration fluctuation equation. The modifications proposed in the past have ranged from ad hoc changes to the constants to development of functional relations for the constants. However, such changes must be tested thoroughly to make them generally applicable to all configurations. Also higher-order Reynolds-stress closure models can be employed. The solution algorithm proposed in this study, because of its attractive numerical properties, can be a viable vehicle for such research activities.

Summary

In this study, an efficient calculation procedure for the solution of the coupled nonlinear partial differential equations governing axisymmetric confined turbulent reacting flows has been developed. The algorithm is an extension of the author's earlier work of calculating isothermal turbulent recirculating flows. Combustion is modeled as a one-step infinite rate reaction, controlled by the turbulent mixing process. A two-equation turbulence model employing transport equations for the kinetic energy of turbulence k and its dissipation rate ϵ is used to represent the turbulent fluxes. For the reacting case, additional equations are solved for the mean and variance of a conserved scalar ξ. Calculations have been made for the experiments of Lockwood et al.[6] for two fuel/air ratios and four finite difference grids of increasing fineness. It is demonstrated that the algorithm, based on the coupled solution of the momentum and continuity equations, is rapidly convergent and has nearly the same efficiency in reacting flows as in nonreacting situations. The calculations are compared with measured mixture fraction distributions.

Acknowledgments

This work was supported by the Ramjet Technology Division, Wright-Patterson AFB, under interagency agreement

with Argonne National Laboratory. The author would like to thank Drs. R. R. Craig and F. D. Stull for their support and encouragement.

References

[1]Edelman, R. B. and Harsha, P. T., "Laminar and Turbulent Gas Dynamics in Combustors—Current Status," *Progress in Energy Combustion and Science*, Vol. 4, 1978, pp. 1-62.

[2]Jones, W. P. and Whitelaw, J. H., "Calculation Methods for Reacting Turbulent Flows: A Review," *Combustion and Flame*, Vol. 48, 1982, pp. 1-26.

[3]Novick, A. S., Miles, G., and Lilley, D. G., "Modeling Parameter Influences in Gas Turbine Combustor Design," *Journal of Energy*, Vol. 3, No. 5, Sept. 1979, pp. 257-262.

[4]Lilley, D. G., "Flowfield Modeling in Practical Combustors: A Review," *Journal of Energy*, Vol. 3, No. 4, July 1979, pp. 193-210.

[5]Mellor, A. M., "Gas Turbine Engine Pollution," *Progress in Energy Combustion Science*, Vol. 1, 1976, pp. 111-133.

[6]Lockwood, F. C., El-Mahallawy, F. M., and Spalding, D. B., "An Experimental and Theoretical Investigation of Turbulent Mixing in a Cylindrical Furnace," *Combustion and Flame*, Vol. 23, 1974, pp. 283-293.

[7]Elgobashi, S., "Studies in the Prediction of Turbulent Diffusion Flames," *Studies in Convection*, Vol. 2, edited by B. E. Launder, Academic Press, New York, 1979, pp. 141-189.

[8]Smith, P. J. and Smoot, L. D., "Turbulent Gaseous Combustion, Part II: Theory and Evaluation for Local Properties," *Combustion and Flame*, Vol. 42, 1981, pp. 277-285.

[9]Hutchinson, P., Khalil, E. E., Whitelaw, J. H., and Wigley, G., "The Calculation of Furnace Flow Properties and Their Experimental Verification," *Journal of Heat Transfer*, Vol. 98, May 1976, pp. 276-283.

[10]Vanka, S. P., Craig, R. R., and Stull, F. D., "Mixing, Chemical Reaction, and Flow Field Development in Ducted Rockets," AIAA Paper 85-1271, July 1985.

[11]Launder, B. E. and Spalding, D. B., "The Numerical Computation of Turbulent Flows," *Computer Methods in Applied Mechanics and Engineering*, Vol. 3, 1974, pp. 269-289.

[12]Spalding, D. B., "Development of the Eddy-Breakup Model of Turbulent Combustion," *The Sixteenth Symposium on Combustion*, The Combustion Institute, Pittsburgh, PA, 1977, pp. 1657-1663.

[13]Patankar, S. V. and Spalding, D. B., "A Calculation Procedure for Three-Dimensional Parabolic Flows," *International Journal of Heat and Mass Transfer*, Vol. 15, Oct. 1972, pp. 1787-1805.

[14]Vanka, S. P., "Computations of Turbulent Recirculating Flows with Fully-Coupled Solution of Momentum and Continuity Equations," *International Journal of Heat and Mass Transfer*, Vol. 28, Nov. 1985, pp. 2093-2103.

[15]Vanka, S. P., "Fully-Coupled Calculation of Fluid Flows with Limited Use of Computer Storage," Argonne National Laboratory, Argonne, IL, Rept. ANL-83-87, 1983.

[16]Bilger, R. W., "Turbulent Flows with Nonpremixed Reactants," *Turbulent Reacting Flows*, edited by P. A. Libby and F. A. Williams, Springer-Verlag, Berlin, 1980, pp. 65-114.

[17]Eisenstat, S. C., Gursky, M. C., Schultz, M. H., and Sherman, A. H., "Yale Sparse Matrix Package: The Non-Symmetric Codes," Yale University, New Haven, CT, Research Rept. 114, 1975.

[18]Sturgess, G. J., "Aerothermal Modeling Program—Phase I Final Report," NASA-CR-168202, 1983.

[19]Srinivasan, R. et al., "Aerothermal Modeling Program—Phase I Final Report," NASA-CR-168243, 1983.

[20]Vanka, S.P., "Calculation of Axisymmetric Turbulent Confined Diffusion Flames," AIAA Paper 85-0141, Jan. 1985.